

Observationally Constrained Cloud Phase Unmasks Orbitally Driven Climate Feedbacks

Navjit Sagoo¹, Trude Storelvmo², Lily Caroline Hahn³, Ivy Tan⁴, James Danco⁵, Bryan Keith Raney⁶, and Anthony J. Broccoli⁶

¹Stockholm University

²University of Oslo

³University of Washington

⁴NASA GSFC

⁵National Weather Service

⁶Rutgers University

November 26, 2022

Abstract

The mechanisms which amplify small orbitally driven changes in insolation and drive the glacial-interglacial cycles of the past 2.7 million years are poorly understood. Previous studies indicate that cloud feedbacks oppose ice sheet initiation at times when orbital configuration supports ice sheet growth. A recent study in which cloud phase was observationally constrained by satellite measurements provides evidence for a weaker opposing cloud feedback than previously found in response to carbon dioxide doubling (Tan et al., 2016). We observationally constrain cloud phase in the Community Earth System Model. We find a weaker cloud phase feedback, which unmasks water vapor and cloud feedbacks that extend cooling to lower latitudes. Snowfall accumulation and ablation metrics also support ice sheet expansion as seen in proxy records. Our results indicate that well understood cloud and water vapor feedbacks are the amplifying mechanism driving orbital climates.

Observationally Constrained Cloud Phase Unmasks Orbitally Driven Climate Feedbacks

N. Sagoo^{1,†}, T. Storelvmo^{1,‡}, L. Hahn^{1,§}, I. Tan^{1,±}, James Danco^{2,#}, Bryan Raney², A.J. Broccoli²

¹Geology & Geophysics Department, Yale University, New Haven, CT 06511, USA

²Department of Environmental Sciences, Rutgers, The State University of New Jersey, New Brunswick, NJ 08901, USA

[†]Department of Meteorology, University of Stockholm, 10691 Stockholm, Sweden

[‡]Department of Geosciences, P.O. Box 1047 Blindern, 0316 Oslo, Norway

[§]Department of Atmospheric Sciences, University of Washington, Seattle, WA 98195, USA

[±]NASA Goddard Space Flight Centre, Greenbelt, MD 20771, USA

[#]National Oceanic and Atmospheric Administration, National Weather Service, Raleigh, NC 27606, USA

Corresponding author: Navjit Sagoo and Lily Hahn (navjit.sagoo@misu.su.se, lchahn@uw.edu)

Key Points:

- The cloud phase feedback is weaker in response to orbital forcing when cloud phase is observationally constrained by satellite data
- Cloud and water vapor feedbacks are identified as mechanisms which amplify orbitally driven solar changes and may lead to glaciation
- Improving cloud phase representation in models is important for understanding the climate system response to forcing in the past climates

1 **Abstract**

2 The mechanisms which amplify small orbitally driven changes in insolation and drive the
3 glacial-interglacial cycles of the past 2.7 million years are poorly understood. Previous studies
4 indicate that cloud feedbacks oppose ice sheet initiation at times when orbital configuration
5 supports ice sheet growth. A recent study in which cloud phase was observationally constrained
6 by satellite measurements provides evidence for a weaker opposing cloud feedback than
7 previously found in response to carbon dioxide doubling (Tan et al., 2016). We observationally
8 constrain cloud phase in the Community Earth System Model. We find a weaker cloud phase
9 feedback, which unmask water vapor and cloud feedbacks that extend cooling to lower
10 latitudes. Snowfall accumulation and ablation metrics also support ice sheet expansion as seen in
11 proxy records. Our results indicate that well understood cloud and water vapor feedbacks are the
12 amplifying mechanism driving orbital climates.

13

14 **Plain Language Summary**

15 The recent ice ages represent large transitions in climate that are forced by small changes in solar
16 radiation, driven by variations in the Earth's orbit. This study aims to identify the mechanisms
17 that amplify this small solar signal and lead to the development of large ice sheets, as this lack of
18 knowledge indicates gaps in our knowledge of the climate system. Cloud phase (the proportion
19 of liquid to ice) is poorly represented in climate models and previous work has shown that this
20 can lead to an underestimation of the climate response to carbon dioxide forcing. This study
21 explores the climate response to orbital forcing when cloud phase is observationally constrained
22 by satellite. Previous modeling studies have found that when high latitude radiation is reduced
23 due to orbital variations, clouds thin, and allow more solar radiation in, effectively opposing the

24 orbital cooling that encourages ice sheet growth. We find that when cloud phase is constrained,
25 this opposing cloud thinning is reduced and cooling extends to lower latitudes via cloud and
26 water vapor feedbacks. Our work indicates that well understood climate processes are the
27 mechanisms that amplify orbital climate forcing, and reiterate the importance in properly
28 simulating cloud phase in climate models.

29

30 **1. Introduction**

31 The Earth has experienced dramatic shifts in climate from glacial to interglacial states
32 during the Pleistocene (the past 2.6 million years), and while these changes are paced by changes
33 in orbital configuration (Hays et al., 1976), there is no satisfactory theory to fully explain how
34 changes in orbit (eccentricity, obliquity and precession) drive ice sheet growth and decay.

35 Milutin Milanković, whose orbital theory is the leading theory today, postulated that changes in
36 Earth's orbit affecting summertime insolation were important in determining global ice volume,
37 and that changes in orbit that led to cooler summers would increase snow and ice preservation
38 (Milanković, 1941). Subsequent work has shown that obliquity is the dominant orbital
39 component recorded in sedimentary archives (Lisiecki & Raymo, 2005; Raymo & Huybers,
40 2008) and may also be the most important control on integrated summer insolation (P. Huybers,
41 2006, 2011; P. J. Huybers & Wunsch, 2005). Obliquity has a large impact on seasonality, with
42 low obliquity resulting in cool summers and warm winters, and vice versa for high obliquity.

43

44 The mean annual radiative forcing associated with high and low obliquity is much too small to
45 directly drive Pleistocene ice sheet growth and decay. Consequently, large amplifying climate
46 feedbacks are required in order to explain the shifts between glacial and interglacial states with

47 orbital forcing. Modeling studies which have incorporated orbital changes and additional climate
48 forcings such as CO₂ (Barnola et al., 1987), dust (Lambert et al., 2008), vegetation and
49 topography have had limited success in both simulating glacial inception or glacial melt (Birch et
50 al., 2017; Dong & Valdes, 1995; Jochum et al., 2012, p. 2; Lambert et al., 2008; Rind et al.,
51 1989) and thus the mechanisms behind orbitally driven ice sheet growth and decay are still
52 poorly understood. A study by Erb et al. (2013) quantified the role of radiative feedbacks to
53 changes in obliquity and found that cloud feedbacks impeded ice sheet initiation by opposing
54 glaciation at times when orbital forcing would otherwise support it. A compensating low cloud
55 feedback has also been identified in other studies (Birch et al., 2017; Jochum et al., 2012)
56 providing an additional complication to understanding the orbit-climate relationship. Jochum et
57 al. (2012) first identified a low cloud feedback which opposed orbital forcing from the last
58 glacial inception (115 kya). They calculated that the initial (orbital) forcing of 1.9 Wm⁻² above
59 60°N was amplified by the snow-ice-albedo feedback by 6.7 Wm⁻² and was damped by a
60 negative cloud feedback of 3.1 Wm⁻², due to a reduction in low cloud. A later study by Birch et
61 al. (2017) which used a high-resolution cloud resolving model to examine the role of clouds in
62 glacial inception found that CRF became less negative in response to insolation at 115 kya,
63 indicating a negative cloud feedback. Clouds are one of the most challenging and uncertain
64 aspects of the climate system (Boucher et al., 2013) and new research suggest that the negative
65 feedback associated with cloud phase changes in existing models may be too strong (Tan et al.,
66 2016).

67

68 Cloud phase is poorly represented in global climate models, which have tended to underestimate
69 the supercooled liquid fraction (SLF) in mixed phase clouds (MPCs) (Cesana et al., 2015;

70 Komurcu et al., 2014). MPCs are common in the mid and high latitudes (Morrison et al., 2012;
71 Shupe, 2011) but are difficult to model for several reasons: there is a paucity of observational
72 data (Illingworth et al., 2007; Morrison et al., 2012) and general difficulties in representing MPC
73 microphysics (Komurcu et al., 2014; Lohmann & Hoose, 2009), in particular the conversion
74 from liquid to ice known as the Wegner-Bergeron-Findeisen (WBF) process (Storelvmo et al.,
75 2008; Tan & Storelvmo, 2016). The cloud phase feedback can be explained as so: in response to
76 warming the liquid-ice phase transition isotherm moves to higher altitudes such that, for a given
77 altitude, the SLF is enhanced relative to the initial state. For a given amount of cloud water,
78 supercooled liquid droplets are more reflective than cloud ice due to their smaller size and larger
79 population (Murray et al., 2012; Pruppacher & Klett, 1978), thus they are more reflective to
80 shortwave (SW) radiation and oppose the initial warming (Mitchell et al., 1989). When SLFs are
81 initially underestimated, this feedback is too strong and masks other cloud processes that
82 generally yield positive feedbacks (Tan et al., 2016). Using observationally constrained cloud
83 phase, Tan et al. (2016) found that the liquid-to-ice transition isotherm moved upward, where
84 there are fewer and thinner clouds, and poleward where incoming solar radiation is reduced.
85 Subsequently the phase transition response to radiative perturbation is weakened and equilibrium
86 climate sensitivity (ECS) increased.

87 This study examines the response of observationally constrained modeled clouds to orbital
88 forcing in pairs of simulations in which obliquity is prescribed at the extremes of its Pleistocene
89 range (Lo and Hi simulations). We quantify radiative feedbacks in response to obliquity forcing
90 in two simulations with the Community Earth System Model (CESM) version 1.0.6 in which
91 SLF is constrained to satellite observations (SLF1 and SLF2). This is compared with both a

92 default (DEF) CESM simulation and corresponding simulations using the GFDL Climate Model,
93 version 2.1 (CM2.1) from Erb et al. (2013).

94 **2. Materials and Methods**

95 *2.1. Climate Model Setup*

96 The Community Earth System Model (CESM) version 1.0.6 (Hurrell et al., 2013) is
97 comprised of the atmospheric component CAM5.1 (Liu et al., 2012; Neale et al., 2010) which
98 has 30 vertical levels and uses the three-mode version of the Modal Aerosol Module (MAM3)
99 (Liu et al., 2012); the Community Land Model (CLM4.0) (Lawrence et al., 2011; Oleson et al.,
100 2010); the ocean model (Parallel Ocean Program Ocean model, POP2) (Smith et al., 2010) and
101 the Ice Model (Community Ice Code, CICE4.0) (Holland et al., 2012; Hunke et al., 2010). In our
102 simulations CAM5.1 and CLM4.0 are run with a resolution of $1.9^\circ \times 2.5^\circ$ whilst POP2 and
103 CICE4.0 have a nominal 1° resolution. The DEF simulation is run with the default cloud
104 microphysics scheme (Morrison & Gettelman, 2008) and the standard ice-nucleation
105 parameterization scheme (Meyers et al., 1992) in which ice nucleating particle number
106 concentration is calculated based on temperature and supersaturation. For the SLF1 and SLF2
107 simulations the ice-nucleation parameterization scheme is updated (DeMott et al., 2015) to a
108 more realistic scheme which enables ice nucleating particle number concentration to be
109 diagnosed as a function of the concentration of large dust particles in addition to temperature.
110 This allows for the spatial and temporal variability of dust IN to be taken into account. As in
111 Tan et al., (2016) SLFs in SLF1 and SLF2 were determined from the results of a 256 member
112 quasi Monte Carlo sampling approach in which six cloud microphysical parameters were
113 modified, and the resulting cloud phase was compared with satellite data from NASA's Cloud-
114 Aerosol-Lidar with Orthogonal Polarization (CALIOP). The parameter combinations selected for

115 SLF1 and SLF2 were very different, but both produced SLFs in excellent agreement with
116 CALIOP.

117 *2.2. Climate Simulations*

118 We use a pre-industrial model configuration (i.e. land mask, ice sheets, greenhouse gases,
119 vegetation and aerosols). Following the methodology of Erb et al. (2013) we perform idealized
120 simulations in which only obliquity is modified to a low (Lo) value of 22.079° and a high (Hi)
121 value of 24.480° representative of the past 600 Kyr. DEF, SLF1 and SLF2 are run with Lo and
122 Hi obliquity (six simulations) for a minimum of 350 years or until the top-of-atmosphere (TOA)
123 energy budget is $< 0.3 \text{ Wm}^{-2}$. These simulations are long enough to capture broad changes in
124 the atmosphere and surface ocean but are not long enough for the oceans to fully respond to the
125 obliquity forcing. The final 50 years of the simulation are used as the input for cloud radiative
126 kernel computations, for calculations of climate means and for the International Satellite Cloud
127 Climatology Project (ISCCP) satellite simulator analysis (Klein & Hartmann, 1993; Webb et al.,
128 2001). All results are presented as Lo-Hi anomalies as this convention reduces northern
129 hemisphere (NH) summer insolation, which is conducive to NH glaciation.

130 *2.3. Downscaling Model*

131 As in Notaro et al. (2014), the downscaling employed the SNOW-17 snow accumulation and
132 ablation model (Anderson 2006), which is used by the United States National Weather Service
133 for real-time hydrologic modeling. SNOW-17 is driven by daily temperature and precipitation.
134 Modern snow cover was simulated on a 1° by 1° latitude-longitude grid by using 30 years of
135 observed daily temperature and precipitation from the data set compiled by Kluver et al. (2016).
136 To simulate snow cover in the low obliquity experiments, a simple bias correction approach is
137 used. For each month, climatological differences in surface air temperature were computed

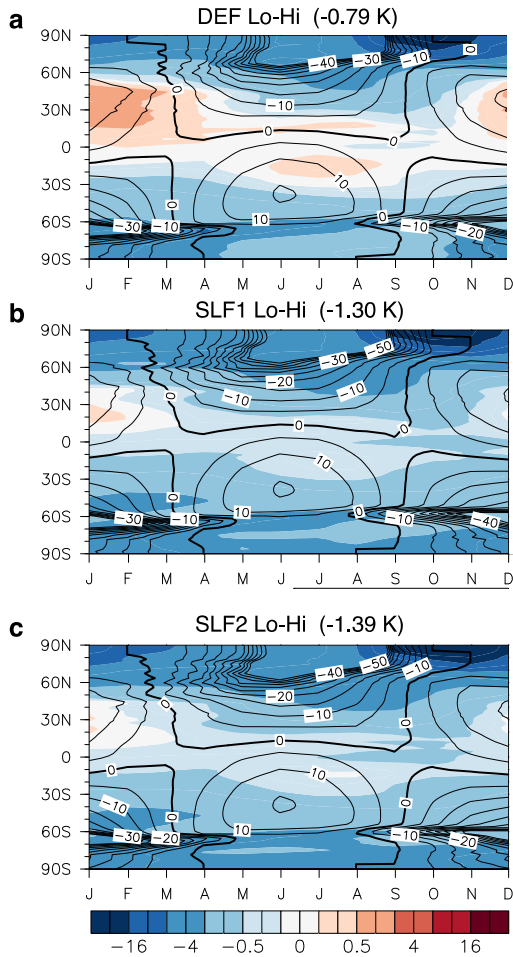
138 between each low obliquity simulation and a corresponding preindustrial simulation with the
139 same cloud parameterization. These differences were interpolated to the 1° by 1° grid and added
140 to the 30-year observed daily temperature time series at each point. A similar approach was used
141 for precipitation except that the ratio of low obliquity and pre-industrial precipitation was
142 determined, and the observed precipitation time series was multiplied by this ratio.

143 **3. Results**

144 *3.1. Temperature and Insolation Seasonal Cycle*

145 Obliquity affects the seasonal cycle of insolation but has a negligible impact on global
146 annual mean insolation, with lower (Lo) obliquity reducing polar insolation in summer and
147 increasing it in winter. Figure 1 shows the annual mean Lo-Hi surface air temperature (SAT)
148 anomaly (colored contours) with the insolation anomaly overlaid (black contours). The negative
149 insolation anomaly (in all simulations) extends across almost all the northern hemisphere (NH)
150 from March to September. In the DEF experiment, negative SAT anomalies lag the insolation
151 anomaly by ~ 6 weeks and have a smaller spatial and temporal extent than the negative
152 anomalies in SLF1 and SLF2. In SLF1 and SLF2 negative SAT anomalies extend equator-wards
153 in March and over the entire NH (and globe) until January where a very small 0.25 K tropical
154 warming occurs.

155 Negative SAT anomalies in SLF1 and SLF2 extend into areas with a positive insolation
156 anomaly and indicate the importance of climate feedbacks over local radiative balance. The Lo-
157 Hi global annual mean SAT anomalies for our experiments are -0.79 K, -1.30 K and -1.36 K for
158 DEF, SLF1 and SLF2 respectively, while in CM2.1 the Lo-Hi anomaly is 0.5 K. These SAT
159 anomalies indicate that the climate response to obliquity forcing is considerably larger when
160 cloud phase is observationally constrained.



161

162 **Figure 1.** Seasonal changes in surface air temperature (SAT) and insolation shown as Lo-Hi
 163 obliquity anomalies. a) DEF, b) SLF1 and c) SLF2. SAT is shown in colored contours with the
 164 global annual mean SAT anomaly value shown at the top of each figure in parenthesis. Overlaid
 165 black contours and labels denote the Lo-Hi insolation anomaly with the thick black line
 166 indicating the zero-insolation contour.

167

168 3.2. Radiative Feedbacks

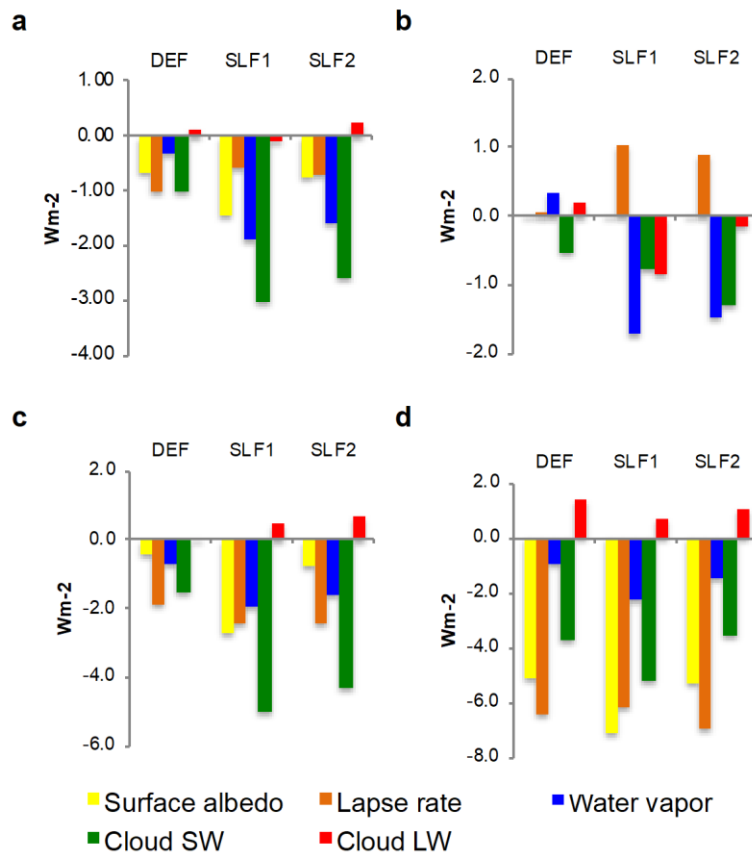
169 We calculate the radiative feedbacks of surface albedo, atmospheric water vapor, vertical
 170 temperature lapse rate and cloud optical properties using the radiative kernel method of climate
 171 feedback analysis (Shell et al., 2008; Soden et al., 2008). Note that results are presented as the
 172 effect of feedbacks on net TOA radiation ΔR_{net} (Wm^{-2}) and not as feedbacks ($\text{Wm}^{-2} \text{K}^{-1}$). A
 173 positive value thus indicates a warming (damping) feedback while a negative value indicates a

174 cooling (amplifying) feedback. Globally, the total feedback is ~1.6 to 1.7 times stronger in SLF1
175 and SLF2 compared to DEF (Figure 2a) and 2.2 to 2.4 times stronger than that found in CM2.1.
176 Both the cloud and water vapor feedbacks are much larger in SLF1 and SLF2 compared to DEF
177 and CM2.1, whilst the lapse rate feedback is similar in all simulations and the surface albedo
178 feedback is only marginally larger in SLF1 and SLF2. When broken down into regions (Figure
179 2b-d) the mid-latitude cloud feedback and tropical water vapor feedback stand out as being much
180 larger in SLF1 and SLF2 compared to DEF.

181 During late summer in the high latitudes low obliquity conditions reduce insolation in
182 this region, which should result in local cooling. Over this period in DEF, column-integrated
183 liquid (liquid water path, LWP) reduces and acts to oppose and reduce cooling from this
184 obliquity driven reduction in insolation (Figure S1). This process is also seen in CM2.1. In the
185 SLF1 and SLF2 simulations this high-latitude LWP reduction in summer is not evident, but a
186 large increase in total (ice+liquid) water path (TWP) appears in the mid-latitudes (30-60°N)
187 which increases cloud reflectivity and thus cooling throughout the year (Figure S1).

188 In response to obliquity forcing (Lo-Hi), cooling leads to cloud liquid being converted to
189 cloud ice, which is optically thinner. The cloud phase bias in DEF causes an exaggerated cloud
190 thinning as too much liquid is converted to ice with cooling. This exaggerated reduction in cloud
191 optical depth counters the other, mainly positive, cloud feedbacks and therefore weakens the
192 spreading of high-latitude cooling to mid- and low latitudes. In contrast, the amplifying mid-
193 latitude cloud feedback in SLF1 and SLF2 is twice as strong as in DEF, permitting high-latitude
194 cooling to spread across the mid-latitudes towards the tropics. The slight cooling in the tropics
195 (as opposed to the warming seen in DEF and CM2.1) is accompanied by a slight decrease in
196 atmospheric water vapor, as expected according to the Clausius-Clapeyron relation. Since water

197 vapor is a potent greenhouse gas, this reduction in water vapor increases outgoing longwave
 198 (LW) radiation and thus constitutes a powerful amplifying feedback in the tropics. The negative
 199 (amplifying) water vapor feedback is enabled by the strong mid-latitude cloud feedback, because
 200 in its absence the summer Lo-Hi insolation anomaly in the tropics, which is slightly positive,
 201 would produce a warming and thus a positive water vapor feedback that would act to oppose to
 202 the orbital forcing (as seen in DEF and in CM2.1).



203

204 **Figure 2.** Radiative feedbacks are partitioned into individual components (surface albedo, lapse
 205 rate, water vapor, cloud shortwave (SW), cloud longwave (LW) and presented for different
 206 regions. a) Global mean; b) low-latitudes (20°S-20°N; c) mid-latitudes (30-60°N and S) and d)
 207 high latitudes (60-90°N and S). Results are presented as the effect of feedbacks on net TOA
 208 radiation (Wm^{-2}) and not as surface temperature-mediated feedbacks ($Wm^{-2} K^{-1}$).

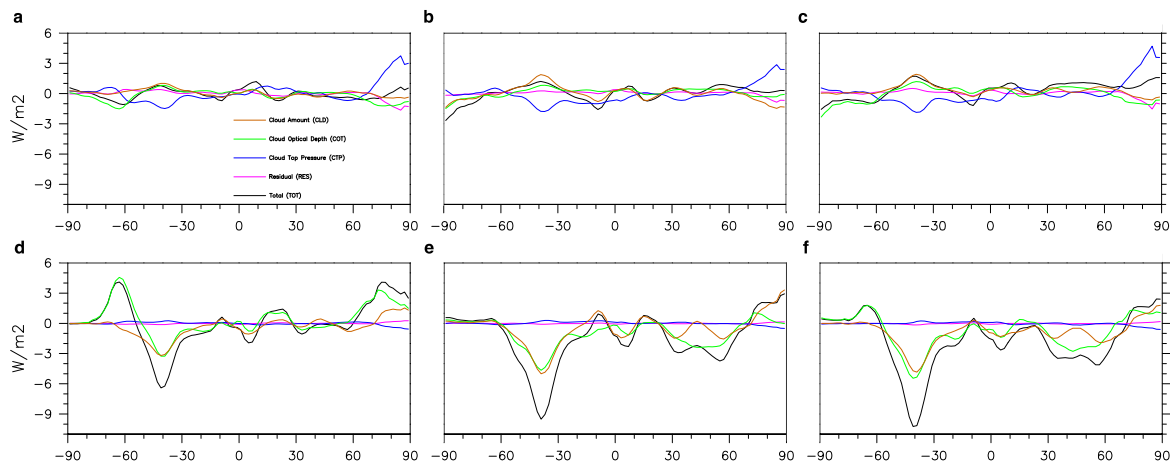
209 *3.3. Decomposing the Cloud (Feedback) Response to Orbital Forcing*

210 In order to more fully understand the changes in cloud properties that occur in response to orbital
211 forcing we examine the output from the International Satellite Cloud Climatology Project
212 satellite simulator (ISCCP) (Klein & Jakob, 1999; Webb et al., 2001) which is implemented in
213 the atmosphere component of CESM, the Community Atmosphere Model (CAM5.1). The
214 ISCCP simulator allows cloud properties in models to be diagnosed in a manner consistent with
215 the satellite view from space. The radiative impact of changes in cloud amount (CLD), optical
216 depth (COT) and cloud top pressure (CTP) as well as a residual term are calculated following
217 Zelinka et al. (2012) and summarized by feedback in Figure 3 with the net feedback shown in
218 Figure S2. This de-composition of the net (SW+LW) cloud feedback into contributions from
219 CLD, CTP and COT reveals that the latter component is responsible for the difference in mid-
220 latitude cloud feedback between DEF on one hand, and SLF1 and SLF2 on the other. Because
221 the orbital signal is strongest in 60-90°N, it helps to consider this region first. In DEF COT is
222 positive whilst in SLF1 and SLF2 it has shifted to less positive values. Now if we consider 60-
223 90°N, COT has decreased from near zero in DEF, to up to -3 Wm^{-2} in SLF1 and SLF2 across this
224 latitude band. This is consistent with the expectation that cloud thinning associated with cloud
225 phase changes should be substantially weakened in the simulations with observationally-
226 constrained SLF.

227 *3.4. Glacial inception*

228 The central tenet of Milanković' orbital theory is that cooler summers allow high latitude snow
229 to survive the summer melt season. Perennial snow cover subsequently leads to snow-albedo
230 feedbacks, which amplify ice cap expansion and initiate the growth of large-scale ice-sheets.
231 Sediment cores indicate that in the NH the last glacial inception occurred $\sim 115,000$ years ago in

232 the region of Hudson Bay and Baffin Island over a period of around 20,000 years (Clark et al.,
 233 1993). We gauge the summer melt response to the cooling signal in these experiments by
 234 calculating the percentage change in positive degree-days (PDD) for the June-July-August (JJA)
 235 period (Figure 4a-c). All three experiments show a substantial reduction in PDD (up to 50%) in
 236 the high Arctic, Hudson Bay area and over Baffin Island, which are likely locations of the last
 237 initiation of the Laurentide ice sheet. In SLF1 and SLF2 the reduction in PDD extends further
 238 into the mid-latitudes than DEF, in agreement with the increased extent of negative SATs.



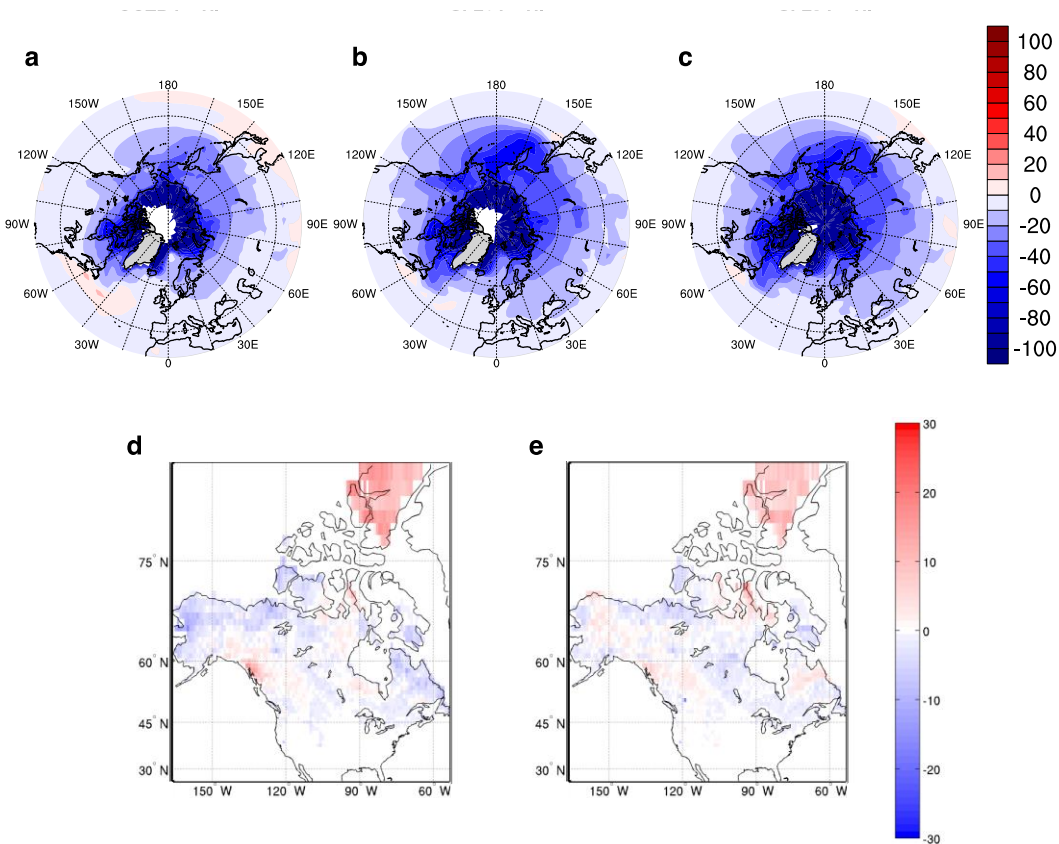
239

240 **Figure 3.** Longwave (LW) and shortwave (SW) cloud feedbacks calculated using the
 241 International Satellite Cloud Climatology Project satellite simulator (ISCCP). LW feedbacks are
 242 shown in the top row: a) DEF, b) SLF1, c) SLF2, SW feedbacks are shown in the bottom row:
 243 d) DEF, e) SLF1 and f) SLF2 with feedbacks due to changes in cloud amount (CLD) shown in
 244 orange, cloud optical depth (COT) in green, cloud top pressure (CTP) in blue, a residual
 245 component in magenta and total feedbacks are shown in black.

246

247 Because climate model resolutions are too coarse to capture the detail required for realistic ice
 248 sheet dynamics (i.e. underlying bedrock topography) (Pollard & Thompson, 1997), a
 249 downscaling approach was also used to determine the extent to which the differences in cloud
 250 parametrization would affect the persistence of snow cover in the low obliquity simulations (see
 251 methods). Figure 4d-e shows the average number of days without snow cover > 1” for the Lo-

252 Preindustrial anomaly over the Canadian Arctic. SLF1 and SLF2 have fewer snow free days over
 253 the summer than DEF, with this increase in snow preservation occurring over the southern part
 254 of Baffin Island, eastwards of the Hudson Bay and over much of northern and middle Canada,
 255 which is in line with the proxy evidence. Because modern simulations were not available for this
 256 study, and the modern climate is warmer than the preindustrial climate, our use of pre-industrial
 257 anomalies likely underestimates the duration of snow cover in the low obliquity experiments.



258

259 **Figure 4.** Indicators of change in summer (June, July, August) snow preservation. Percentage
 260 change in positive-degree days (PDD) polewards of 30°N for northern hemisphere for Lo-Hi
 261 anomaly shown for a) DEF, b) SLF1 and c) SLF2 Lo-Hi experiments with blue indicating fewer
 262 PDD and increased likelihood of snow preservation. A downscaling model was used to calculate
 263 the average number of days without snow $\geq 1''$ in the Canadian Arctic for the Lo-Pre-industrial
 264 anomaly for DEF, SLF1 and SLF2. The anomaly of d) SLF1-DEF and e) SLF2-DEF are shown
 265 in the bottom row where blue indicates an increase in snow covered days.

266

267 **4. Discussion and Conclusions**

268 We have repeated the experiments in Erb et al. (2013) to examine the obliquity driven
269 climate response in a model with observationally constrained supercooled liquid fraction (SLF)
270 in mixed phase clouds (MPCs). SLFs are increased in two experiments (SLF1 and SLF2) using a
271 more realistic ice-nucleation scheme (DeMott et al., 2015) but using different methods in order
272 to account for the uncertainties associated with MPC microphysics. These are compared with a
273 default model (DEF) in which SLFs are known to be underestimated (Cesana et al., 2015;
274 Komurcu et al., 2014). Other studies have found that orbitally induced climate changes are
275 opposed by reductions in high latitude low level cloud (Birch et al., 2017; Erb et al., 2013;
276 Jochum et al., 2012). However, when realistic SLFs are used, this negative cloud feedback is
277 reduced which allows obliquity-driven cooling to spread to lower latitudes. This cooling leads to
278 an increased liquid water path (LWP) and ice water path (IWP) in mid-latitude clouds and this
279 positive cloud feedback further extends the cooling signal both throughout the year and leads to a
280 strong tropical water vapor feedback. Overall the SAT response in SLF1 and SLF2 is 2-3 times
281 larger than that in CM2.1 whilst the sum of radiative feedbacks are 1.6 - 2.3 times larger in SLF1
282 and SLF2 compared with DEF and CM2.1. Reductions in positive degree days (PDDs) of up to
283 50% occur in the summer melt season in the Hudson Bay and Baffin Island area which have
284 been identified as probable locations for the expansion of the Laurentide ice sheet (Clark et al.,
285 1993). These and further reductions in PDD which extend into the mid-latitudes in SLF1 and
286 SLF2, and reduction in snow-free days calculated from the downscaling approach provide
287 further support that the climate in these experiments is more conducive to ice-sheet growth. The
288 processes that contribute to the extension and expansion of the cooling signal are the same in

289 both hemispheres unlike other studies in which only a strong northern hemisphere signal is
290 simulated (Jochum et al., 2012).

291 Simulating cloud processes is a challenging area of study and it should be noted that the
292 microphysics that contribute to high SLFs in mixed phase clouds are not completely understood:
293 both reductions in the efficiency of the Wegner-Bergeron-Findeisen (WBF) process (Lohmann &
294 Hoose, 2009; Storelvmo et al., 2008; Tan & Storelvmo, 2016) and the availability, size
295 distribution and effectiveness of ice nucleating particles such as mineral dust (Atkinson et al.,
296 2013; Kok et al., 2017; Murray et al., 2012; Sagoo & Storelvmo, 2017) have a significant impact
297 on SLFs and climate. The positive feedbacks which amplify the orbital signal in this work were
298 only unmasked because the high latitude negative cloud feedback was not present in SLF1 and
299 SLF2. Understanding the response of low Arctic clouds to changes in climate and sea-ice cover
300 is challenging (Kay et al., 2011; Kay & Gettelman, 2009) and thus the magnitude and even the
301 presence of a high latitude summer low cloud feedback are still not well constrained. Finally, in
302 summary, we find strong support for Milanković's orbital theory in this study when SLFs are
303 observationally constrained. Enhanced cooling in the high latitudes leads to the unmasking of
304 well-known positive mid-latitude cloud feedbacks and tropical water vapor feedback, which
305 amplify the obliquity signal by additional cooling which reduces summer snow/ice melt.

306 **Acknowledgments, Samples, and Data**

- 307 • Simulations were run on the Yale High Performance Computing Cluster.
- 308 • CESM model output for this study is available at <http://doi.org/10.5281/zenodo.3891912>.
- 309 • The authors declare no competing interests.

310 **Author contributions**

311 A.B conceived the project, A.B, T.S and N.S designed and organized this study. L.H, N.S, T.S,
312 A.B carried out the analysis. J.D and B.R developed the downscaling software and made the
313 calculations. L.H, N.S and T.S wrote the manuscript. All authors discussed and contributed to the
314 manuscript.

315 **References**

- 316 Atkinson, J. D., Murray, B. J., Woodhouse, M. T., Whale, T. F., Baustian, K. J., Carslaw, K. S.,
317 et al. (2013). The importance of feldspar for ice nucleation by mineral dust in mixed-
318 phase clouds. *Nature*, 498(7454), 355–358.
- 319 Barnola, J.-M., Raynaud, D., Korotkevich, Y. S., & Lorius, C. (1987). Vostok ice core provides
320 160,000-year record of atmospheric CO₂. *Nature*, 329(6138), 408–414.
- 321 Birch, L., Cronin, T., & Tziperman, E. (2017). Glacial Inception on Baffin Island: The Role of
322 Insolation, Meteorology, and Topography. *Journal of Climate*, 30(11), 4047–4064.
323 <https://doi.org/10.1175/JCLI-D-16-0576.1>
- 324 Boucher, O., Randall, D., Artaxo, P., Bretherton, C., Feingold, G., Forster, P., et al. (2013).
325 Clouds and Aerosols: In Climate Change 2013: The Physical Science Basis Contribution
326 of Working Group I to the Fifth Assessment Report of the Intergovernmental Panel on
327 Climate Change. K., Tignor, M., Allen, SK, Boschung, J., Nauels, A., Xia, Y., Bex, V.,
328 Midgley, PM, Eds.
- 329 Cesana, G., Waliser, D. E., Jiang, X., & Li, J.-L. (2015). Multimodel evaluation of cloud phase
330 transition using satellite and reanalysis data. *Journal of Geophysical Research:*
331 *Atmospheres*, 120(15), 7871–7892.
- 332 Clark, P. U., Clague, J. J., Curry, B. B., Dreimanis, A., Hicock, S. R., Miller, G. H., et al. (1993).
333 Initiation and development of the Laurentide and Cordilleran ice sheets following the last
334 interglaciation. *Quaternary Science Reviews*, 12(2), 79–114.
- 335 DeMott, P. J., Prenni, A. J., McMeeking, G. R., Sullivan, R. C., Petters, M. D., Tobo, Y., et al.
336 (2015). Integrating laboratory and field data to quantify the immersion freezing ice
337 nucleation activity of mineral dust particles. *Atmospheric Chemistry and Physics*, 15(1),
338 393–409.

- 339 Dong, B., & Valdes, P. J. (1995). Sensitivity studies of Northern Hemisphere glaciation using an
340 atmospheric general circulation model. *Journal of Climate*, 8(10), 2471–2496.
- 341 Erb, M. P., Broccoli, A. J., & Clement, A. C. (2013). The contribution of radiative feedbacks to
342 orbitally driven climate change. *Journal of Climate*, 26(16), 5897–5914.
- 343 Hays, J. D., Imbrie, J., Shackleton, N. J., & others. (1976). Variations in the Earth's orbit:
344 pacemaker of the ice ages. American Association for the Advancement of Science.
345 Retrieved from
346 [https://www.researchgate.net/profile/J_Hays/publication/301325552_Variations_in_the_](https://www.researchgate.net/profile/J_Hays/publication/301325552_Variations_in_the_Earth_pacemaker_of_the_ice_ages/links/573cca0c08ae9ace840fe240.pdf)
347 [Earth_pacemaker_of_the_ice_ages/links/573cca0c08ae9ace840fe240.pdf](https://www.researchgate.net/profile/J_Hays/publication/301325552_Variations_in_the_Earth_pacemaker_of_the_ice_ages/links/573cca0c08ae9ace840fe240.pdf)
- 348 Holland, M. M., Bailey, D. A., Briegleb, B. P., Light, B., & Hunke, E. (2012). Improved sea ice
349 shortwave radiation physics in CCSM4: the impact of melt ponds and aerosols on Arctic
350 sea ice*. *Journal of Climate*, 25(5), 1413–1430.
- 351 Hunke, E. C., Lipscomb, W. H., Turner, A. K., & others. (2010). CICE: the Los Alamos Sea Ice
352 Model Documentation and Software User's Manual Version 4.1 LA-CC-06-012. *T-3*
353 *Fluid Dynamics Group, Los Alamos National Laboratory*, 675. Retrieved from
354 <http://oceans11.lanl.gov/svn/CICE/tags/release-5.1/doc/cicedoc.pdf>
- 355 Hurrell, J. W., Holland, M. M., Gent, P. R., Ghan, S., Kay, J. E., Kushner, P. J., et al. (2013).
356 The community earth system model: a framework for collaborative research. *Bulletin of*
357 *the American Meteorological Society*, 94(9), 1339–1360.
- 358 Huybers, P. (2006). Early Pleistocene glacial cycles and the integrated summer insolation
359 forcing. *Science*, 313(5786), 508–511.
- 360 Huybers, P. (2011). Combined obliquity and precession pacing of late Pleistocene deglaciations.
361 *Nature*, 480(7376), 229–232.

- 362 Huybers, P. J., & Wunsch, C. (2005). Obliquity pacing of the late Pleistocene glacial
363 terminations. Retrieved from <https://dash.harvard.edu/handle/1/3382978>
- 364 Illingworth, A. J., Hogan, R. J., O'connor, E. J., Bouniol, D., Delanoë, J., Pelon, J., et al. (2007).
365 Cloudnet: Continuous evaluation of cloud profiles in seven operational models using
366 ground-based observations. *Bulletin of the American Meteorological Society*, 88(6), 883–
367 898.
- 368 Jochum, M., Jahn, A., Peacock, S., Bailey, D. A., Fasullo, J. T., Kay, J., et al. (2012). True to
369 Milankovitch: Glacial inception in the new community climate system model. *Journal of*
370 *Climate*, 25(7), 2226–2239.
- 371 Kay, J. E., & Gettelman, A. (2009). Cloud influence on and response to seasonal Arctic sea ice
372 loss. *Journal of Geophysical Research: Atmospheres*, 114(D18), D18204.
373 <https://doi.org/10.1029/2009JD011773>
- 374 Kay, J. E., Holland, M. M., & Jahn, A. (2011). Inter-annual to multi-decadal Arctic sea ice extent
375 trends in a warming world. *Geophysical Research Letters*, 38(15), L15708.
376 <https://doi.org/10.1029/2011GL048008>
- 377 Klein, S. A., & Hartmann, D. L. (1993). The Seasonal Cycle of Low Stratiform Clouds. *Journal*
378 *of Climate*, 6(8), 1587–1606. [https://doi.org/10.1175/1520-](https://doi.org/10.1175/1520-0442(1993)006<1587:TSCOLS>2.0.CO;2)
379 [0442\(1993\)006<1587:TSCOLS>2.0.CO;2](https://doi.org/10.1175/1520-0442(1993)006<1587:TSCOLS>2.0.CO;2)
- 380 Klein, S. A., & Jakob, C. (1999). Validation and sensitivities of frontal clouds simulated by the
381 ECMWF model. *Monthly Weather Review*, 127(10), 2514–2531.
- 382 Kluver, D., Mote, T., Leathers, D., Henderson, G. R., Chan, W., & Robinson, D. A. (2016).
383 Creation and validation of a comprehensive 1 by 1 daily gridded North American dataset

384 for 1900–2009: Snowfall. *Journal of Atmospheric and Oceanic Technology*, 33(5), 857–
385 871.

386 Kok, J. F., Ridley, D. A., Zhou, Q., Miller, R. L., Zhao, C., Heald, C. L., et al. (2017). Smaller
387 desert dust cooling effect estimated from analysis of dust size and abundance. *Nature*
388 *Geoscience*, 10(4), 274–278. <https://doi.org/10.1038/ngeo2912>

389 Komurcu, M., Storelvmo, T., Tan, I., Lohmann, U., Yun, Y., Penner, J. E., et al. (2014).
390 Intercomparison of the cloud water phase among global climate models. *Journal of*
391 *Geophysical Research: Atmospheres*, 119(6), 2013JD021119.
392 <https://doi.org/10.1002/2013JD021119>

393 Lambert, F., Delmonte, B., Petit, J.-R., Bigler, M., Kaufmann, P. R., Hutterli, M. A., et al.
394 (2008). Dust-climate couplings over the past 800,000 years from the EPICA Dome C ice
395 core. *Nature*, 452(7187), 616–619.

396 Lawrence, D. M., Oleson, K. W., Flanner, M. G., Thornton, P. E., Swenson, S. C., Lawrence, P.
397 J., et al. (2011). Parameterization improvements and functional and structural advances in
398 Version 4 of the Community Land Model. *Journal of Advances in Modeling Earth*
399 *Systems*, 3(1), M03001. <https://doi.org/10.1029/2011MS00045>

400 Lisiecki, L. E., & Raymo, M. E. (2005). A Pliocene-Pleistocene stack of 57 globally distributed
401 benthic $\delta^{18}\text{O}$ records. *Paleoceanography*, 20(1). Retrieved from
402 <http://onlinelibrary.wiley.com/doi/10.1029/2004PA001071/full>

403 Liu, X., Easter, R. C., Ghan, S. J., Zaveri, R., Rasch, P., Shi, X., et al. (2012). Toward a minimal
404 representation of aerosols in climate models: Description and evaluation in the
405 Community Atmosphere Model CAM5. *Geoscientific Model Development*, 5(3), 709.

- 406 Lohmann, U., & Hoose, C. (2009). Sensitivity studies of different aerosol indirect effects in
407 mixed-phase clouds. *Atmospheric Chemistry and Physics*, 9(22), 8917–8934.
- 408 Meyers, M. P., DeMott, P. J., & Cotton, W. R. (1992). New primary ice-nucleation
409 parameterizations in an explicit cloud model. *Journal of Applied Meteorology*, 31(7),
410 708–721.
- 411 Milanković, M. (1941). *Kanon der Erdbestrahlung und seine Anwendung auf das*
412 *Eiszeitenproblem*. na.
- 413 Mitchell, J. F., Senior, C. A., & Ingram, W. J. (1989). CO₂ and climate: a missing feedback?
414 *Nature*, 341(6238), 132–134.
- 415 Morrison, H., & Gettelman, A. (2008). A New Two-Moment Bulk Stratiform Cloud
416 Microphysics Scheme in the Community Atmosphere Model, Version 3 (CAM3). Part I:
417 Description and Numerical Tests. *Journal of Climate*, 21(15), 3642–3659.
418 <https://doi.org/10.1175/2008JCLI2105.1>
- 419 Morrison, H., de Boer, G., Feingold, G., Harrington, J., Shupe, M. D., & Sulia, K. (2012).
420 Resilience of persistent Arctic mixed-phase clouds. *Nature Geoscience*, 5(1), 11–17.
421 <https://doi.org/10.1038/ngeo1332>
- 422 Murray, B. J., O’Sullivan, D., Atkinson, J. D., & Webb, M. E. (2012). Ice nucleation by particles
423 immersed in supercooled cloud droplets. *Chemical Society Reviews*, 41(19), 6519–6554.
- 424 Neale, R. B., Chen, C.-C., Gettelman, A., Lauritzen, P. H., Park, S., Williamson, D. L., et al.
425 (2010). Description of the NCAR community atmosphere model (CAM 5.0). *NCAR*
426 *Tech. Note NCAR/TN-486+ STR*. Retrieved from
427 https://www.cesm.ucar.edu/models/ccsm4.0/cam/docs/description/cam4_desc.pdf

- 428 Notaro, M., Lorenz, D., Hoving, C., & Schummer, M. (2014). Twenty-first-century projections
429 of snowfall and winter severity across central-eastern North America. *Journal of Climate*,
430 27(17), 6526–6550.
- 431 Oleson, K. W., Lawrence, D. M., Gordon, B., Flanner, M. G., Kluzek, E., Peter, J., et al. (2010).
432 Technical description of version 4.0 of the Community Land Model (CLM). Retrieved
433 from <http://citeseerx.ist.psu.edu/viewdoc/summary?doi=10.1.1.172.7769>
- 434 Pollard, D., & Thompson, S. L. (1997). Driving a high-resolution dynamic ice-sheet model with
435 GCM climate: ice-sheet initiation at 116 000 BP. *Annals of Glaciology*, 25, 296–304.
- 436 Pruppacher, H. R., & Klett, J. D. (1978). Microphysics of clouds and precipitation. *Reidel*,
437 *Dordrecht, Holland, 714pp.*
- 438 Raymo, M. E., & Huybers, P. (2008). Unlocking the mysteries of the ice ages. *Nature*,
439 451(7176), 284–285.
- 440 Rind, D., Peteet, D., & Kukla, G. (1989). Can Milankovitch orbital variations initiate the growth
441 of ice sheets in a general circulation model? *Journal of Geophysical Research:*
442 *Atmospheres*, 94(D10), 12851–12871.
- 443 Sagoo, N., & Storelvmo, T. (2017). Testing the sensitivity of past climates to the indirect effects
444 of dust. *Geophysical Research Letters*, 44(11), 2017GL072584.
445 <https://doi.org/10.1002/2017GL072584>
- 446 Shell, K. M., Kiehl, J. T., & Shields, C. A. (2008). Using the radiative kernel technique to
447 calculate climate feedbacks in NCAR's Community Atmospheric Model. *Journal of*
448 *Climate*, 21(10), 2269–2282.
- 449 Shupe, M. D. (2011). Clouds at Arctic atmospheric observatories. Part II: Thermodynamic phase
450 characteristics. *Journal of Applied Meteorology and Climatology*, 50(3), 645–661.

- 451 Smith, R., Jones, P., Briegleb, B., Bryan, F., Danabasoglu, G., Dennis, J., et al. (2010). The
452 parallel ocean program (POP) reference manual ocean component of the community
453 climate system model (CCSM) and community earth system model (CESM). *Rep. LAUR-*
454 *01853, 141*, 1–140.
- 455 Soden, B. J., Held, I. M., Colman, R., Shell, K. M., Kiehl, J. T., & Shields, C. A. (2008).
456 Quantifying climate feedbacks using radiative kernels. *Journal of Climate*, *21*(14), 3504–
457 3520.
- 458 Storelvmo, T., Kristjánsson, J. E., Lohmann, U., Iversen, T., Kirkevåg, A., & Seland, Ø.
459 (2008). Modeling of the Wegener–Bergeron–Findeisen process—implications for aerosol
460 indirect effects. *Environmental Research Letters*, *3*(4), 045001.
- 461 Tan, I., & Storelvmo, T. (2016). Sensitivity study on the influence of cloud microphysical
462 parameters on mixed-phase cloud thermodynamic phase partitioning in CAM5. *Journal*
463 *of the Atmospheric Sciences*, *73*(2), 709–728.
- 464 Tan, I., Storelvmo, T., & Zelinka, M. D. (2016). Observational constraints on mixed-phase
465 clouds imply higher climate sensitivity. *Science*, *352*(6282), 224–227.
- 466 Webb, M., Senior, C., Bony, S., & Morcrette, J.-J. (2001). Combining ERBE and ISCCP data to
467 assess clouds in the Hadley Centre, ECMWF and LMD atmospheric climate models.
468 *Climate Dynamics*, *17*(12), 905–922.
- 469 Zelinka, M. D., Klein, S. A., & Hartmann, D. L. (2012). Computing and partitioning cloud
470 feedbacks using cloud property histograms. Part I: Cloud radiative kernels. *Journal of*
471 *Climate*, *25*(11), 3715–3735.



Geophysical Research Letters

Supporting Information for

Observationally Constrained Cloud Phase unmasks Orbitally Driven Climate Feedbacks

N. Sagoo^{1,†}, T. Storelvmo^{1,‡}, L. Hahn^{1,§}, I. Tan^{1,±}, James Danco^{2,#}, Bryan Raney², A.J. Broccoli²

¹Geology & Geophysics Department, Yale University, New Haven, CT 06511, USA

²Department of Environmental Sciences, Rutgers, The State University of New Jersey, New Brunswick, NJ 08901, USA

[†]Department of Meteorology, University of Stockholm, 10691 Stockholm, Sweden

[‡]Department of Geosciences, P.O. Box 1047 Blindern, 0316 Oslo, Norway

[§]Department of Atmospheric Sciences, University of Washington, Seattle, WA 98195, USA

[±]NASA Goddard Space Flight Centre, Greenbelt, MD 20771, USA

[#]National Oceanic and Atmospheric Administration, National Weather Service, Raleigh, NC 27606, USA

Contents of this file

Text S1

Figures S1 to S2

Table S1

Text S1

Supplementary Methods

The “SLF1” and “SLF2” simulations in this study are based on the “CALIOP-SLF1” and “CALIOP-SLF2” simulations from Tan et al., 2016, in which modeled supercooled liquid fraction (SLF) were matched to observational data. The original simulations had a small cool bias and so we modified the cloud tuning values in these simulations in order to improve the climate (Table S1).

We use a pre-industrial model configuration (i.e. land mask, ice sheets, greenhouse gases, vegetation and aerosols). Following the methodology of Erb et al., 2013, we perform idealized simulations in which only obliquity is modified to a low (Lo) value of 22.079° and a high (Hi) value of 24.480° representative of the past 600 Kyr. DEF, SLF1 and SLF2 are run with Lo and Hi obliquity (six simulations) for a minimum of 350 years or until the top-of-atmosphere (TOA) energy budget is $> 0.3 \text{ Wm}^{-2}$. These simulations are long enough to capture broad changes in the atmosphere and surface ocean but are not long enough for the oceans to fully respond to the obliquity forcing. The final 50 years of the simulation are used for climate computations. All results are presented as Lo-Hi anomalies as this convention reduces northern hemisphere (NH) summer insolation, which is conducive to NH glaciation.

Figure S1. Figure S1. Seasonal variations in column-integrated liquid and ice presented as Lo-Hi anomalies for total grid box. Column 1 shows DEF, column 2 SLF1 and column 3 SLF2 for a-c) cloud liquid water path (LWP), d-f) ice water path (IWP) and g-j) total cloud water path (TWP). Units are g/m^2 .

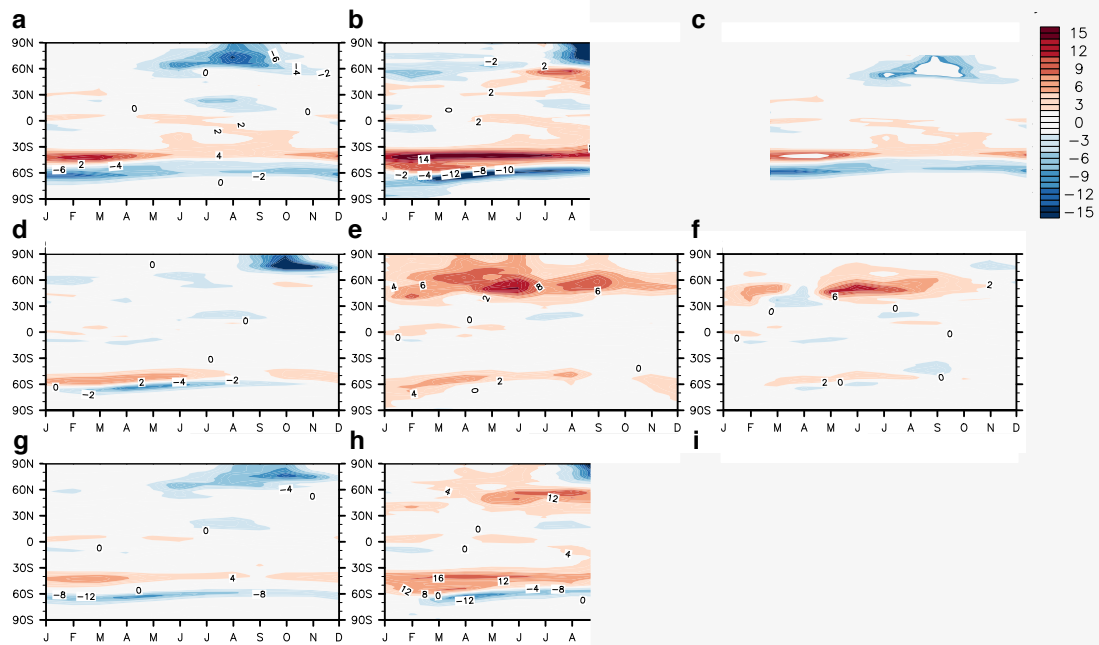


Figure S2. Net cloud feedbacks calculated using the International Satellite Cloud Climatology Project satellite simulator (ISCCP). a) DEF, b) SLF1 and c) SLF2. Feedbacks due to changes in cloud amount (CLD) are shown in orange, cloud optical depth (COT) in green, cloud top pressure (CTP) in blue, a residual component (RES) in magenta and total feedbacks (TOT) shown in black.

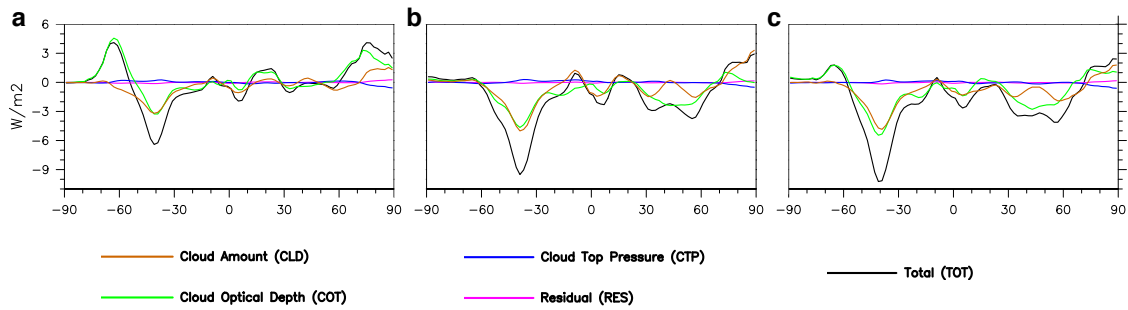


Table S1. Tuning values used for simulations presented in this work. Our values are shown in bold. Values used in Tan et al., 2016 are shown in italics and default values shown in parenthesis

	SLF1	SLF2
rhminl	0.9175 (0.8) <i>0.8725</i>	0.8925 (0.8) <i>0.8475</i>
rhminh	0.8 (0.8) <i>0.8</i>	0.99 (0.8) <i>0.99</i>